Measuring stiffness and residual stress of thin films by contact resonance atomic force microscopy

2016 Appl. Phys. Express 9 116601

(http://iopscience.iop.org/1882-0786/9/11/116601)

Applied Physics Express **9**, 116601 (2016)
http://doi.org/**10.7567/APEX.9.116601**

Measuring stiffness and residual stress of thin films by contact resonance atomic force microscopy

Chengfu Ma[1,2], Yuhang Chen[1*], Jianfeng Chen[1,2], and Jiaru Chu[1]

[1]*Department of Precision Machinery and Precision Instrumentation, University of Science and Technology of China, Hefei, Anhui 230026, China*
[2]*USTC Center for Micro- and Nanoscale Research and Fabrication, University of Science and Technology of China, Hefei, Anhui 230026, China*

*E-mail: chenyh@ustc.edu.cn

Received August 1, 2016; accepted September 14, 2016; published online October 6, 2016

A method based on contact resonance atomic force microscopy (AFM) was proposed to determine the mechanical properties of thin films. By analyzing the contact resonance frequencies of an AFM probe while the tip was in contact with the sample, the stiffness and residual stress of a freestanding circular SiN_x membrane were evaluated quantitatively. The obtained magnitude of residual stress was in reasonable agreement with that determined by wafer curvature measurement. The method was verified to have much better mechanical sensitivity than the popular AFM bending test method. Its promising application to fast, nondestructive mechanical mapping of thin-film-type structures at the nanoscale was also demonstrated.

With the rapid development of nanoscience and nanotechnology, thin films have been extensively applied in a wide range of fields, including micro-electromechanical systems, sensors and actuators, and optical devices.[1–4] Among their many characteristics of concern, the mechanical properties are of fundamental importance to device performance. Therefore, there is an urgent demand for developing fast, nondestructive, and quantitative characterization methods. Unfortunately, because of the different thermal expansion coefficients between the deposited material and the substrate, residual stress is common in prepared thin films, greatly affecting their mechanical behaviors and making their characterization more challenging.[5] To measure the mechanical properties of thin films, especially the residual stress, several techniques have been developed, such as wafer curvature measurement,[6] the bugle test,[7] nanoindentation,[8] resonance-based techniques,[9] and the X-ray method.[10] In the case of two-dimensional (2D) material films and nanowire beams, the atomic force microscopy (AFM) static point-deflection method is attracting more and more attention owing to its ultrahigh force and displacement resolutions.[11,12] However, only by utilizing a probe having a matching force constant with the stiffness of the investigated film can satisfactory accuracy be acquired.

Acoustic-based AFM techniques, in which contact-mode AFM is combined with ultrasonic-frequency vibrations, have emerged as powerful tools for the mechanical characterization of materials in the past two decades. Such techniques have already been successfully applied to study the elastic properties of advanced materials, detect subsurface defects and nanostructures, and explore interface characteristics.[13–16] Especially, by recording the contact resonance (CR) frequencies and subsequently performing analysis with a proper tip–sample contact model and cantilever dynamic model, quantitative mechanical characterizations can be realized with CR-AFM techniques. However, most such investigations focused on the evaluation of the elastic modulus or stiffness, and few publications have concerned the residual stress until now. In this letter, we proposed a new method of studying the mechanical properties, especially the residual stress, of thin films by CR-AFM techniques. The stiffness distribution of a freestanding circular SiN_x membrane was first measured. Then, the residual stress was evaluated by modeling the mechanics of a prestressed circular membrane under a point load. The obtained residual stress was in reasonable agreement with that determined by the wafer curvature test. The method was verified to have a much better mechanical response sensitivity than the quasi-static AFM bending test method. Its capability for fast, nondestructive mechanical mapping at the nanoscale was also demonstrated, making it quite appealing, especially for applications to nanofilms with irregular shapes, heterogeneous mechanical properties, or defects.

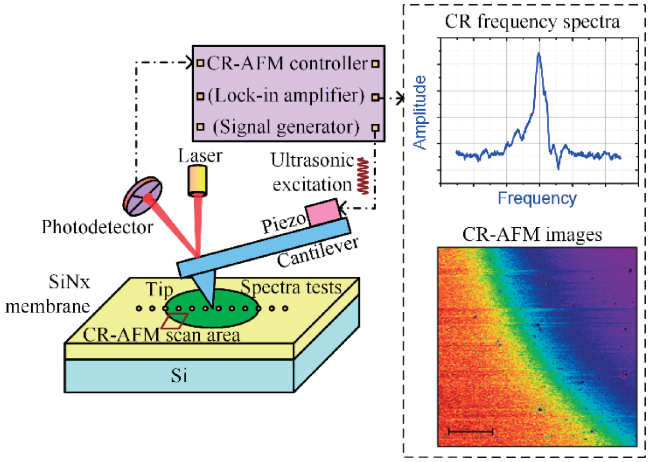

Fig. 1. Schematic illustration of using CR-AFM for the mechanical characterization of a freestanding circular thin film.

The schematic illustration of exploiting CR-AFM for the mechanical characterization of thin films is shown in Fig. 1. The following experiments were performed on a commercial AFM platform (Asylum Research MFP-3D Origin) with the ultrasonic excitation applied to the probe, which is the so-called ultrasonic-AFM (UAFM) mode.[17] By recording the CR spectra with the lock-in amplifier under a sweeping frequency excitation, CR frequencies at different positions on the membrane, which are relevant to local stiffness and modulus, can be obtained. Additionally, by oscillating the probe around one of the CR frequencies while the tip is scanning the surface, and by extracting the amplitude and phase signals, a qualitative mechanical mapping of the membrane can be realized. Furthermore, with the aid of techniques such as Dual AC™ Resonance Tracking (DART),[18] a CR frequency image can also be easily acquired, which can be quantitatively converted into maps of corresponding mechanical properties.

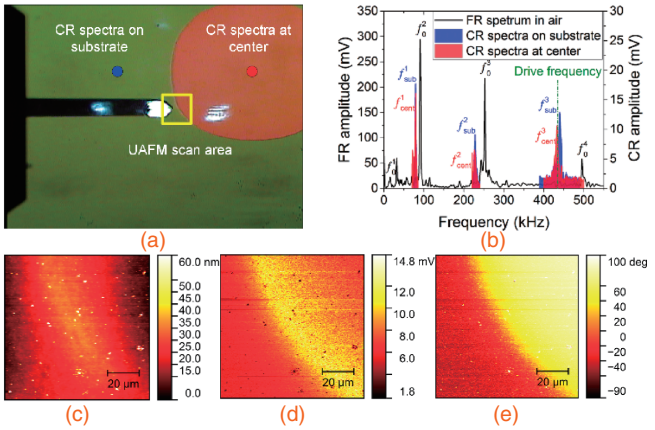

Fig. 2. (a) Optical view of the cantilever and membrane sample showing CR spectroscopy test positions and the UAFM scan area. (b) Frequency spectra in air, in contact with the substrate and at the membrane center. (c)–(e) UAFM topography, amplitude, and phase images.

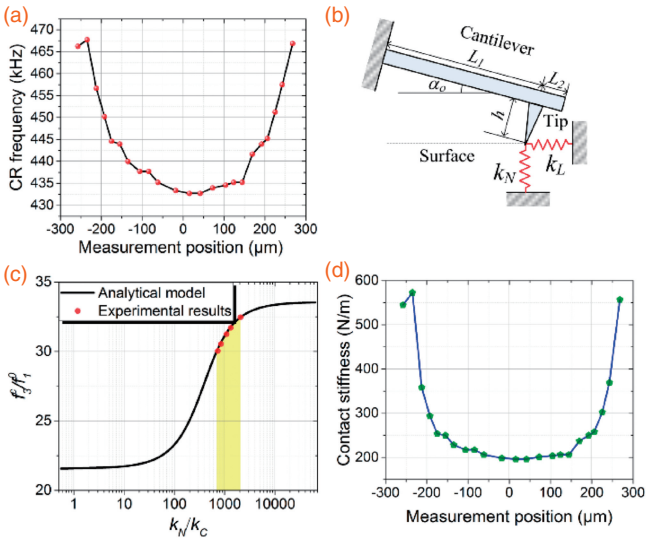

Fig. 3. (a) Extracted 3rd CR frequencies under various positions along the radial direction. (b) Simplified analytical model of the cantilever in contact with the sample. (c) Relationship between the normalized 3rd CR frequency and the normalized contact stiffness. The experimentally obtained CR frequencies are marked on the curve. (d) Calculated contact stiffness values.

A thin clamped freestanding circular SiN_x membrane was fabricated to test the method, by the process described in Fig. S1 in the online supplementary data at http://stacks.iop.org/APEX/9/116601/mmedia. The measurements started with a demonstration of the mechanical characterization ability based on CR-AFM. The tested membrane was determined to have a thickness of 524 ± 0.9 nm after a wafer-scale measurement with a film thickness mapping tool (Angstrom Sun Technologies SRM300) and a diameter of about 504 μm using an optical microscope. As shown in the optical view in Fig. 2(a), a ContAl-G cantilever (Innovative Solutions Bulgaria BudgetSensors) was first brought into contact with the sample surface, and then CR spectroscopy and UAFM imaging were applied. Before the measurements, the inverse optical lever sensitivity was determined to be 157.6 nm/V and the spring constant of the cantilever to be 0.28 N/m by thermal calibration.[19] The first four free resonance (FR) frequencies of the cantilever were 14.4, 91.6, 252.6, and 495.1 kHz. All experiments were conducted under a tip load of approximately 88 nN.

Then CR spectra tests were conducted on the substrate and at the membrane center area. As shown in Fig. 2(b), the first three CR frequencies were around 79, 230, and 450 kHz. It can be unambiguously seen that there was a much larger frequency shift for the third CR eigenmode than for the first and second modes, where the frequency at the center was smaller than that on the substrate. Actually, compared with those on the substrate, the first three CR frequencies at the center were, respectively, almost the same, and approximately 8 kHz smaller and 35 kHz smaller (see Fig. S2 in the online supplementary data at http://stacks.iop.org/APEX/9/116601/mmedia). This indicates that the second and third CR modes have considerably better sensitivities, where the latter had the best sensitivity, to the mechanical difference between the solid substrate and the freestanding membrane. Consequently, the third CR mode was chosen in the following experiments. Next, to demonstrate the mechanical mapping capability of CR-AFM, a UAFM scan was applied with the drive frequency set at 440 kHz around the third CR frequency. Figures 2(c)–2(e) show the obtained topography, amplitude, and phase images in the $90 \times 90\,\mu m^2$ scan area around the membrane periphery. It can be seen that, from the amplitude and phase images, the freestanding membrane can be unambiguously distinguished from the substrate, which was not possible from the topography.

To characterize the stiffness distribution of the membrane, CR spectra were swept at different positions along its radial axis, as illustrated in Fig. 1. Figure 3(a) shows the third CR frequencies extracted from these spectra. There is a bowl-shaped distribution along the membrane's radial direction, indicating that the membrane center area has the lowest stiffness, and there is a rapid increase in the stiffness while moving toward the periphery.

A simplified analytical model of the cantilever in contact with the sample, as schematically shown in Fig. 3(b), was used to convert the measured CR frequencies to contact stiffness values. Both the normal and lateral contact interactions (represented by k_N and k_L, respectively), the cantilever tilt of α_0 induced by the mounting angle of the cantilever holder, and the tip position (L_1, L_2) and height h were considered. The characteristic Euler–Bernoulli equation describing the transverse flexural vibration of the cantilever is

$$EI\frac{\partial^4 y(x,t)}{\partial x^4} + \rho A\frac{\partial^2 y(x,t)}{\partial t^2} = 0, \quad (1)$$

where E is Young's modulus, I is the area moment of inertia, ρ is the mass density, and A is the sectional area. $y(x,t)$ denotes the cantilever deflection, and the general solution is in the form of

$$y(x,t) = (a_1 e^{\lambda x} + a_2 e^{-\lambda x} + a_3 e^{i\lambda x} + a_4 e^{-i\lambda x})e^{i\omega t}. \quad (2)$$

Here, ω is the angular frequency and λ is the wave number. The constant parameters a_1, a_2, a_3, and a_4 can be determined from the boundary conditions. First, the deflection and the slope are zero at the clamped end. Second, no moment or shear force is present at the free end. Last, the tip–sample interactions k_N and k_L induce corresponding shear force and bending moment, and the deflection and slope should be continuous for the two cantilever sections L_1 and L_2 at the tip position. By combining the characteristic equation and the boundary conditions, the contact stiffness is computed by numerically solving[20]

$$\frac{C}{3}\frac{k_C}{k_N} + B_1 + B_2\frac{k_L}{k_N} + 3A\frac{k_L}{k_N}\frac{k_N}{k_C} = 0, \tag{3}$$

where

$$A = \left(\frac{h}{L_1}\right)^2 (1 - \cos\lambda_n L_1 \cosh\lambda_n L_1) \times (1 + \cos\lambda_n L_2 \cosh\lambda_n L_2), \tag{4}$$

$$B_1 = \sin^2\alpha_0 B_1^* - B_2^* + \cos^2\alpha_0 B_3^*, \tag{5}$$

$$B_2 = \cos^2\alpha_0 B_1^* + B_2^* + \sin^2\alpha_0 B_3^*, \tag{6}$$

$$C = 2(\lambda_n L_1)^4 (1 + \cos\lambda_n L \cosh\lambda_n L), \tag{7}$$

with

$$B_1^* = \left(\frac{h}{L_1}\right)^2 (\lambda_n L_1)^3 \times [(1 + \cos\lambda_n L_2 \cosh\lambda_n L_2)(\sin\lambda_n L_1 \cosh\lambda_n L_1 + \cos\lambda_n L_1 \sinh\lambda_n L_1) - (1 - \cos\lambda_n L_1 \cosh\lambda_n L_1) \times (\sin\lambda_n L_2 \cosh\lambda_n L_2 + \cos\lambda_n L_2 \sinh\lambda_n L_2)], \tag{8}$$

$$B_2^* = \left(\frac{h}{L_1}\right)(\lambda_n L_1)^2 \sin\alpha_0 \cos\alpha_0 \times [(1 + \cos\lambda_n L_2 \cosh\lambda_n L_2)\sin\lambda_n L_1 \sinh\lambda_n L_1 + (1 - \cos\lambda_n L_1 \cosh\lambda_n L_1)\sin\lambda_n L_2 \sinh\lambda_n L_2], \tag{9}$$

$$B_3^* = \lambda_n L_1 \times [(1 + \cos\lambda_n L_2 \cosh\lambda_n L_2)(\sin\lambda_n L_1 \cosh\lambda_n L_1 - \cos\lambda_n L_1 \sinh\lambda_n L_1) - (1 - \cos\lambda_n L_1 \cosh\lambda_n L_1) \times (\sin\lambda_n L_2 \cosh\lambda_n L_2 - \cos\lambda_n L_2 \sinh\lambda_n L_2)]. \tag{10}$$

Here, $\lambda_n L$ is the normalized wave number of the nth flexural resonance eigenmode and can be related to the CR frequency f_n^c and the FR frequency f_n^0 from the dispersion equation as follows (the superscripts c and 0 respectively denote the CR and FR modes here):

$$(\lambda_n L)^c = (\lambda_n L)^0 \sqrt{\frac{f_n^c}{f_n^0}}. \tag{11}$$

In our experiments, the cantilever length L is 450 μm and the tip has a height of 17 μm and a position L_1/L of 0.9667, as provided by the manufacturer. The cantilever tilt angle is 11°. The contact stiffness ratio k_L/k_N is estimated to be equal to $2(1-\nu)/(2-\nu)$ on the supported substrate, which yields 0.84 for a material with a Poisson's ratio ν of 0.27.[21] By substituting the measured CR frequencies on the substrate area into Eq. (3) with k_L/k_N set to be 0.84, a mean value of 468.9 N/m was determined for k_L. As k_L will remain constant across the entire measurement, the normal contact stiffness values on the membrane can be calculated with k_L set to be 468.9 N/m.

Figure 3(c) shows the calculated relation between the third CR frequency and the normal contact stiffness respectively normalized by the first FR frequency and the cantilever spring constant. When we marked the experimental CR frequencies on this curve, a good sensitivity of the third mode was again demonstrated. Then contact stiffness values were calculated from the corresponding experimental CR frequencies and the results are shown in Fig. 3(d). The obtained contact stiffness along the membrane's radial direction also has a bowl-shaped distribution, with the magnitudes ranging from about 558 N/m on the substrate to about 196 N/m at the membrane center.

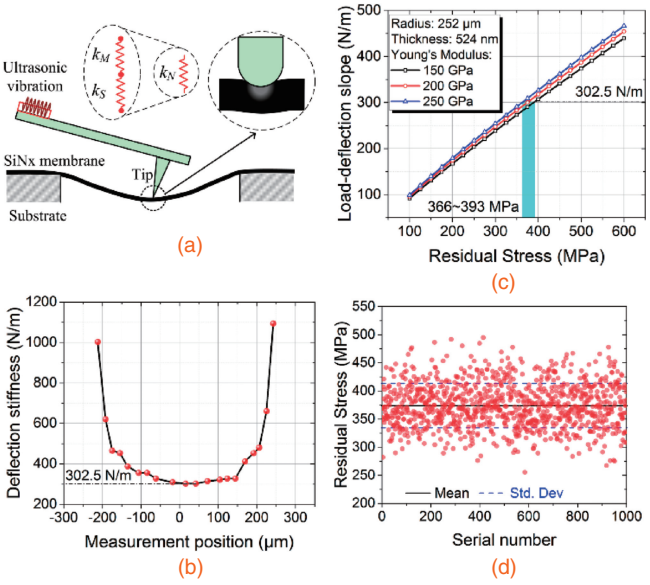

Fig. 4. (a) Schematic illustration of the vibrated cantilever in contact with the membrane. (b) Obtained deflection stiffness values at various positions along the radial direction of the membrane. (c) Calculated stiffness values at the membrane center with various residual stresses and Young's moduli. (d) Values of the residual stress calculated one thousand times in uncertainty analysis.

Then, the stiffness of the membrane was calculated by considering the model of a vibrating cantilever in contact with a membrane, as shown in Fig. 4(a). Overall deflection of the membrane (structure) and local deformation of the material (material) occur during the measurement, both of which are assumed to be elastic under such small loading forces. Therefore, the contact stiffness k_N can be regarded as a series of membrane deflection stiffness k_S and material deformation stiffness k_M, that is, $1/k_N = 1/k_S + 1/k_M$. Since there is no membrane deflection on the substrate area, that is, $k_S \to \infty$, we obtain $(1/k_N = 1/k_M)_{substrate}$. This leads to $(1/k_S)_{membrane} = (1/k_N)_{membrane} - (1/k_N)_{substrate}$. Thus, by assigning $(k_N)_{membrane}$ to be the mean contact stiffness obtained on the substrate area, the membrane stiffness $(k_S)_{membrane}$ can be evaluated from previously calculated contact stiffness values. Figure 4(b) shows the derived membrane stiffness at various positions along the radial direction, indicating a minimum stiffness of 302.5 N/m at the center and a sharp increase around the periphery. Such a large stiffness of the membrane strongly implies the existence of tensile residual stress.

To determine the residual stress of the membrane, the modeling of the mechanics of a prestressed circular membrane is necessary. The deflection at the center of a circular membrane under a vertical point load P at the center and a radial tensile force per unit length N at the edge can be expressed as[22]

$$w = \frac{PR^2}{16\pi D} g(k), \tag{12}$$

where

$$g(k) = \frac{8}{k^2}\left\{\frac{\left[K_1(k) - \frac{1}{k}\right]}{I_1(k)}[I_0(k) - 1] + K_0(k) + \ln\left(\frac{k}{2}\right) + \gamma\right\}, \tag{13}$$

Table I. Parameters and their mean values and deviations considered in the uncertainty analysis.

	Mean value	Deviation
Cantilever length L (μm)	450	±10
Tip position L_1/L	0.9667	±0.0111
Tip height h (μm)	17	±2
Cantilever tilt α_0 (deg)	11	±2
Cantilever stiffness k_C (N/m)	0.28	±0.014
First FR frequency f_1^0 (kHz)	14.4	±0.5
CR frequencies f_n^c (kHz)	—	±2
Membrane radius R (μm)	252	±10
Membrane thickness t (nm)	524	±5
Young's modulus E (GPa)	200	±50
Poisson's ratio ν	0.27	±0.02

and $D = Et^3/12(1-\nu^2)$ is the flexural rigidity of the membrane, with E being Young's modulus, t the thickness, and ν Poisson's ratio. $k^2 = NR^2/D$ is a defined coefficient with R being the membrane radius. I_0 and I_1 are the modified Bessel functions of the first kind of order 0 and 1, and K_0 and K_1 are those of the second kind of order 0 and 1, respectively; γ is Euler's constant. Thus, the stiffness of a circular membrane at the center, that is, the load-deflection slope P/w, is determined by the radius R, the thickness t, the Young's modulus E, and the residual stress σ ($\sigma = N/t$). Figure 4(c) shows the calculated center stiffness values of membranes with various residual stresses and Young's moduli. In the calculation, the radius and thickness were fixed at 252 μm and 524 nm, respectively. It can be found that the membrane stiffness increases dramatically with increasing residual stress. However, the stiffness is much less sensitive to Young's modulus. This makes it possible to determine the residual stress sufficiently accurately by adopting a reasonable assumption of Young's modulus. Here, Young's modulus of the tested SiN_x membrane was set within 150–250 GPa, which is the range of most frequently reported values in the literature for thin films made by the same fabrication process.[23,24] Then, by matching the calculated load-deflection slopes with the obtained membrane stiffness at the center, 302.5 N/m, the residual stress was finally determined to be in the range of 366–393 MPa.

In addition, a thorough uncertainty analysis of our method was performed. All the experimental and model parameters were considered in the analysis by adopting random deviations with sufficiently large ranges for them, as listed in Table I. Then the calculations of the residual stress were repeated one thousand times, and the results are shown in Fig. 4(d). A mean value of 374 MPa and a standard deviation of 39 MPa were determined for the residual stress, indicating the good stability of the method.

The experimental results indicate that the developed tests based on CR-AFM spectroscopy can be used to characterize the stiffness and residual stress of thin films simultaneously. The method was first compared with the quasi-static AFM-based bending test. Force-displacement tests were performed in-situ during the CR spectroscopy experiments. Unlike the 2nd- and 3rd-mode CR spectra, the results show that the AFM bending tests cannot even distinguish the freestanding membrane, as demonstrated in Fig. S2. That is, the CR method has much better mechanical sensitivity. Then, the obtained residual stress was compared with that determined by the widely used wafer curvature test on another SiN_x membrane fabricated under the same processing conditions but with a slight difference in the film thickness. A stylus profiler system (Bruker Dektak XT) was used to measure the residual stress, and an average stress of 372 MPa with a standard deviation of about 59 MPa within an 80-mm-long profile was obtained (see Fig. S3 in the online supplementary data at http://stacks.iop.org/APEX/9/116601/mmedia). This ascertains that the acquired residual stress of 366–393 MPa is in reasonable agreement with that obtained by the conventional wafer curvature test.

In summary, a method based on CR-AFM techniques was proposed to study the stiffness distribution and residual stress of a freestanding circular SiN_x membrane. The method was demonstrated to have much better mechanical sensitivity than the popular quasi-static AFM bending test. The obtained residual stress value was verified to be in good agreement with that obtained by the wafer curvature test. In addition, the ability of CR-AFM for fast, nondestructive mechanical mapping of thin films at the nanoscale was also demonstrated. This paves the way for the simultaneous measurements of the modulus, stiffness, and residual stress of thin films at the nanoscale. CR-AFM has potential applications in film-based micro- and nanodevices, including those of 2D materials.

Acknowledgments This work was financially supported by research grants (Nos. 51275503 and 51675504) from the National Natural Science Foundation of China. The authors acknowledge the technical support from the USTC Center for Micro- and Nanoscale Research and Fabrication.

1) Y. Fu, H. Du, W. Huang, S. Zhang, and M. Hu, Sens. Actuators A **112**, 395 (2004).
2) K. Lee, R. Gatensby, N. McEvoy, T. Hallam, and G. S. Duesberg, Adv. Mater. **25**, 6699 (2013).
3) C. C. Striemer, T. R. Gaborski, J. L. McGrath, and P. M. Fauchet, Nature **445**, 749 (2007).
4) C. Reinhardt, T. Müller, A. Bourassa, and J. C. Sankey, Phys. Rev. X **6**, 021001 (2016).
5) C. C. Lee, G. Z. Cao, and I. Y. Shen, Sens. Actuators A **159**, 88 (2010).
6) C. A. Klein, J. Appl. Phys. **88**, 5487 (2000).
7) E. I. Bromley, J. N. Randall, D. C. Flanders, and R. W. Mountain, J. Vac. Sci. Technol. B **1**, 1364 (1983).
8) G. M. Pharr and W. C. Oliver, MRS Bull. **17** [7], 28 (1992).
9) S. Ma, S. Wang, F. Iacopi, and H. Huang, Appl. Phys. Lett. **103**, 031603 (2013).
10) U. Welzel, J. Ligot, P. Lamparter, A. C. Vermeulen, and E. J. Mittemeijer, J. Appl. Crystallogr. **38**, 1 (2005).
11) Y. Calahorra, O. Shtempluck, V. Kotchetkov, and Y. E. Yaish, Nano Lett. **15**, 2945 (2015).
12) Y. Gao, Y. J. Sun, and T. Y. Zhang, Appl. Phys. Lett. **108**, 123104 (2016).
13) T. Tsuji and K. Yamanaka, Nanotechnology **12**, 301 (2001).
14) G. S. Shekhawat and V. P. Dravid, Science **310**, 89 (2005).
15) D. C. Hurley, M. Kopycinska-Müller, E. D. Langlois, A. B. Kos, and N. Barbosa, III, Appl. Phys. Lett. **89**, 021911 (2006).
16) Z. Parlak, Q. Tu, and S. Zauscher, Nanotechnology **25**, 445703 (2014).
17) C. Ma, Y. Chen, T. Wang, and J. Chu, Scanning **37**, 284 (2015).
18) A. Gannepalli, D. G. Yablon, A. H. Tsou, and R. Proksch, Nanotechnology **22**, 355705 (2011).
19) J. E. Sader, J. W. Chon, and P. Mulvaney, Rev. Sci. Instrum. **70**, 3967 (1999).
20) D. C. Hurley and J. A. Turner, J. Appl. Phys. **102**, 033509 (2007).
21) P. E. Mazeran and J. L. Loubet, Tribology Lett. **7**, 199 (1999).
22) S. Hong, T. P. Weihs, J. C. Bravman, and W. D. Nix, J. Electron. Mater. **19**, 903 (1990).
23) H. Huang, K. J. Winchester, A. Suvorova, B. R. Lawn, Y. Liu, X. Z. Hu, J. M. Dell, and L. Faraone, Mater. Sci. Eng. A **435–436**, 453 (2006).
24) J. A. Taylor, J. Vac. Sci. Technol. A **9**, 2464 (1991).